Magnetic structures of erbium under high pressure

1993 J. Phys.: Condens. Matter 5 1535

(http://iopscience.iop.org/0953-8984/5/10/011)

J. Phys.: Condens. Matter 5 (1993) 1535–1546. Printed in the UK

Magnetic structures of erbium under high pressure

S Kawano†, B Lebech‡ and N Achiwa§

† Research Reactor Institute, Kyoto University, Kumatori, Sennan, Osaka 590-04, Japan
‡ Department of Solid State Physics, Risø National Laboratory, DK-4000, Roskilde, Denmark
§ Physics Department, Faculty of Science, Kyushu University, Hakozaki, Fukuoka 812, Japan

Received 16 November 1992, in final form 21 December 1992

Abstract. Neutron diffraction studies of the magnetic structures of erbium metal at 4.5 K and 11.5 kbar hydrostatic pressure have revealed that the transition to a conical structure at low temperatures is suppressed and that the cycloidal structure, with modulation vector $Q \simeq (\frac{2}{7}2\pi/c)\hat{c}$ persists down to 4.5 K. The existence of higher-harmonic magnetic satellites indicates that the cycloid is squared up. Preliminary data at higher temperatures show that the cycloidal structure changes to a longitudinally modulated structure at $\sim$ 50 K and that the modulation vector remains unchanged between 4.5 K and $\sim$ 50 K, where it tends to increase. The intensities of the magnetic satellites originating from *higher-order harmonics of the c-axis-moment component observed at 4.5 K decrease* slowly with increasing temperature, but persist up to $\sim$ 60 K.

1. Introduction

The various oscillatory, cycloidal or helical orderings of the magnetic moment observed in rare earth metals and their alloys are the result of a compromise between competing magnetic interactions such as the Ruderman–Kittel–Kasuya–Yoshida (RKKY) interaction, one-ion and two-ion anisotropy effects, and magnetoelastic effects (Jensen and Mackintosh 1991). The dependence of the magnetic structures on interatomic distance should provide information on these competing interactions and lead us to a deeper understanding of the transitions between the observed kaleidoscopic spin configurations. Therefore, high-pressure studies have been performed on the rare earth metals (McWhan and Stevens 1965, Robinson *et al* 1966, Wazzan *et al* 1967 and Milton and Scott 1967). However, most of these studies used measurements of electrical resistance or initial permeability and the detailed magnetic structures under pressure have not so far been extensively investigated. Umebayashi *et al* (1968) have carried out neutron diffraction studies of the effects of pressure on Tb and Ho in the limited pressure–temperature range from 0 to 6 kbar between 80 and 300 K. In Er metal, the magnetic transition temperatures are much lower than those in Tb and Ho. Until rather recently, high-pressure neutron scattering investigations have not been achievable at these low temperatures. Accordingly, no neutron diffraction study of the effect of pressure on the magnetic structures of Er has been performed. Recently, Onodera *et al* (1987) have developed a McWhan-type (McWhan *et al* 1974) high-pressure cell for neutron scattering and have used it to examine pressure effects on the magnetic structures of Ho (Achiwa *et al* 1988) and Tb

0953-8984/93/101535+12$07.50

(Kawano *et al* 1992) over a wide pressure and temperature range (from 0 to 25 kbar and from 10 to 300 K) by neutron diffraction. In this paper, we present the results of a neutron diffraction study of the magnetic structures of Er under high pressure by means of a high-pressure cell similar to the one mentioned above.

2. Experimental details

An almost cube-shaped Er single crystal ($3 \times 3 \times 4$ mm^3) was mounted in the high-pressure cell (Onodera *et al* 1987) so that the [1 0 0] axis was vertical. The Er sample was placed in the cell on top of a single crystal of NaCl. For the appropriate crystal orientations, diffraction peaks from either the Er sample or the NaCl crystal could be observed because of the finite height and large vertical divergence of the neutron beam. In this way, the pressure could be monitored during the diffraction experiment by measuring the dependence of the NaCl lattice parameter on the hydrostatic pressure applied to the sample. In the present investigation the pressure was clamped at 11.5 kbar and remained constant throughout the data collection. The pressure cell was mounted on the cold tip of a variable temperature He^4 cryostat which was placed on the sample table of the spectrometer. The neutron diffraction experiments were carried out at Risø National Laboratory, Denmark, using the TAS6 spectrometer operating in the two-axis mode. The incident neutron wavelength of 2.453 Å was selected by means of the (0 0 2) reflection from a pyrolytic-graphite monochromator. The higher-order-wavelength contamination of the incident beam was removed by means of a pyrolytic-graphite filter which was placed in the beam after the monochromator. The collimations from source to monochromator, monochromator to sample and sample to detector were 100, 30 and 30 minutes, respectively. The data were collected for the (h h ℓ)-type reflections and the diffracted intensities were normalized to constant monitor counts by means of a neutron-beam monitor inserted in the incident beam between the pyrolytic-graphite filter and the sample.

3. Results and discussion

Figure 1 shows neutron diffraction patterns obtained for scans along the (0 0 ℓ) direction at 11.5 kbar. Figure 1(a) was measured at 95 K, i.e. well above the Néel temperature, and figure 1(b) at 4.5 K. The difference between the two patterns is shown in figure 1(c). The pattern at 95 K shows only the (0 0 2) nuclear reflection from Er and in addition several powder peaks from the inner part of the hot-pressed Al_2O_3 cylinder which serves as the pressure supporting device. Figure 1(c) thus shows the magnetic reflections at 4.5 K which arise only from the magnetic ordering of moment components perpendicular to the c-axis. No higher-harmonic magnetic satellites are observed in the (0 0 ℓ) diffraction pattern. Figure 2 shows similar diffraction patterns for scans along the (1 1 ℓ) direction at 11.5 kbar at 95 K (figure 2(a)), 4.5 K (figure 2(b)) and the difference between them (figure 2(c)). It is obvious from figure 2(c) that higher-harmonic satellites up to the fifth, as well as an apparent ferromagnetic moment component overlapping with the (1 1 0) and (1 1 2) nuclear reflections, are observed. For clarity, the difference patterns are also shown on a log-intensity scale in figure 3. It should be emphasized that the data

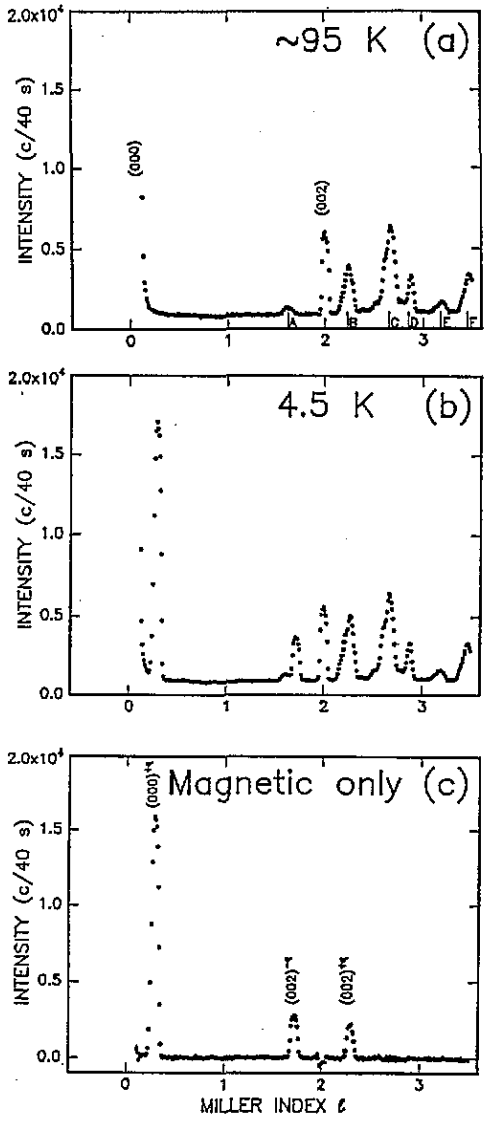

Figure 1. Diffraction patterns for Er at 11.5 kbar hydrostatic pressure obtained by scanning along the [0 0 ℓ] direction (c^*-axis). Figures 1(*a*) and 1(*b*) show the patterns obtained at 95 K, i.e. well above the Néel temperature, and at 4.5 K, respectively. Figure 1(*c*) shows the difference between (*a*) and (*b*), i.e. only the magnetic scattering. The Miller indices for the nuclear Bragg peaks and for the first-order magnetic satellite peaks are shown in (*a*) and (*c*), respectively. The peaks marked A, B, C, D, E and F (in (*a*)) correspond to the (0 1 2), (1 0 4), (1 1 0), (1 1 3), (2 0 2) and (0 2 4) and reflections (hexagonal cell) from the Al_2O_3 pressure-supporting device. The Miller indices $(h\ k\ \ell)^{+nq}$ or $(h\ k\ \ell)^{-nq}$ refer to magnetic satellites at $(h\ k\ \ell+nq)$ or $(h\ k\ \ell-nq)$, respectively. The intensities have been normalized to constant monitor counts (see text).

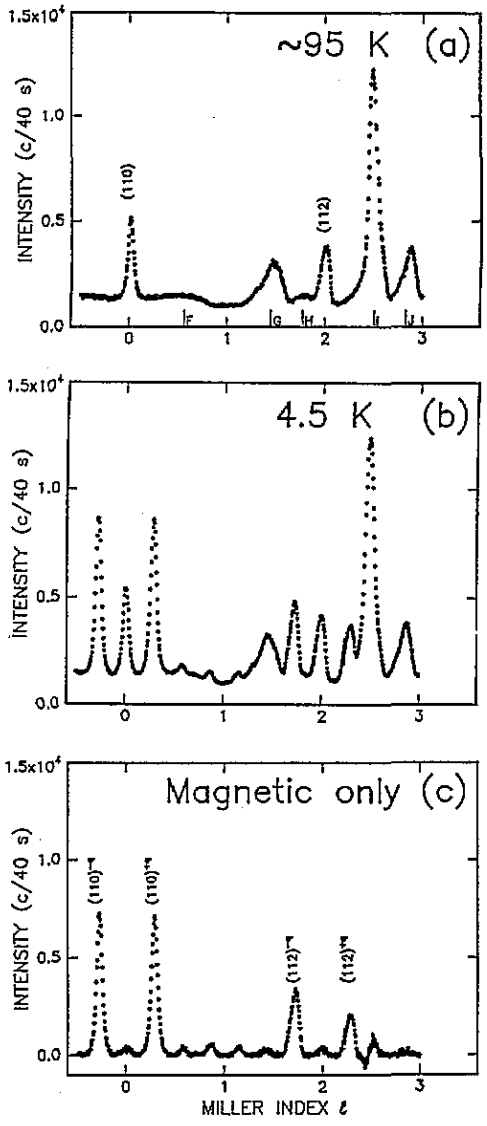

Figure 2. Diffraction patterns for Er at 11.5 kbar hydrostatic pressure obtained by scanning along the [1 1 ℓ] direction. Figures 2(*a*) and 2(*b*) show the patterns obtained at 95 K, i.e. well above the Néel temperature, and at 4.5 K, respectively. Figure 2(*c*) shows the difference between (*a*) and (*b*), i.e. only the magnetic scattering. The Miller indices for the nuclear Bragg peaks and for the first-order magnetic satellite peaks are shown in (*a*) and (*c*), respectively. The peaks marked F, G, H, I and J (in (*a*)) correspond to the (0 2 4), (1 1 6), (2 1 1), (2 1 4) and (0 3 0) reflections (hexagonal cell) from the Al_2O_3 pressure-supporting device. The Miller indices $(h\ k\ \ell)^{+nq}$ or $(h\ k\ \ell)^{-nq}$ refer to magnetic satellites at $(h\ k\ \ell+nq)$ or $(h\ k\ \ell-nq)$, respectively. The intensities have been normalized to constant monitor counts (see text).

in figures 1, 2 and 3 have been normalized to constant monitor counts although the ordinates in these figures are marked counts per 40 seconds for illustrative purposes. The modulation wave-vector of the oscillation of the c-axis component is found to be $q = 0.286 \simeq 2/7$ at 4.5 K. This fact means that the apparent ferromagnetic moment component is equivalent to the seventh-harmonic moment component of the pressure-induced modulated magnetic order in Er. Because no higher-order satellites were observed in the $(0\ 0\ \ell)$ direction (see figure 1(c)), the third, fifth, and seventh harmonic moment components originate predominantly from moment components aligned parallel to the c-axis.

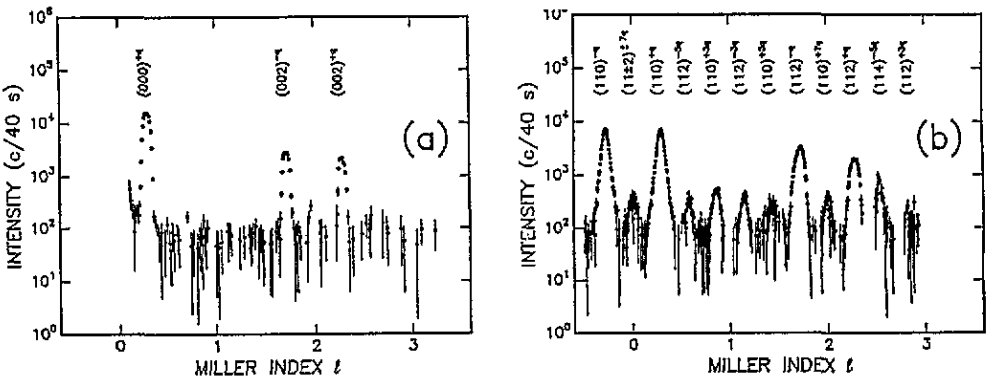

Figure 3. Magnetic satellite peaks in Er at 4.5 K and at 11.5 kbar hydrostatic pressure for neutron diffraction scans along [0 0 ℓ] (upper panel, (a)) and along [1 1 ℓ] (lower panel, (b)). The intensity is on a log scale and the data points are the same as those shown in figures 1(c) and 2(c). However, data points for which the statistical uncertainties exceed the actual difference counts have been excluded. Satellites up to seventh order are observed in the scan along [1 1 ℓ] while only first-order satellites are observed in the scan along [0 0 ℓ]. The Miller indices $(h\ k\ l)^{+nq}$ or $(h\ k\ l)^{-nq}$ refer to magnetic satellites at $(h\ k\ \ell+nq)$ or $(h\ k\ \ell - nq)$, respectively. The intensities have been normalized to constant monitor counts (see text).

As the temperature is decreased, Er metal exhibits three distinct magnetic phase transitions at ambient pressure (Habenschuss *et al* 1974, Atoji 1974). The easy axis in Er is the c-axis and the moments order into a c-axis longitudinally modulated structure at $T_N = 84.4$ K. As the temperature is reduced, the structure gradually squares up. Below $T_{CY} = 52.4$ K, the moment component perpendicular to the c-axis begins to order, and finally at $T_C = 18$ K, a first-order transition to a narrow cone is observed. This cone has an opening angle of $\sim 30°$ and a modulation vector $q \simeq 5/21$. Although the neutron diffraction patterns for a three-domain cycloidal structure and a c-axis modulated helical structure are essentially indistinguishable in the presence of random domains, Jensen and Mackintosh (1991) have argued that, in the temperature interval from T_C to T_{CY}, the most probable ordering of the moments in Er is an almost planar elliptic cycloidal structure with the moments close to the ac-plane; a result which also agrees with the mean field calculations by Jensen (1976). Because the magnetoelastic effects play an important role in the transition from the cycloidal structure to the cone with a ferromagnetic c-axis moment component, it is expected that application of hydrostatic pressure could suppress the cone phase

(Jensen and Mackintosh 1991). The present investigations show that the temperature induced transition from the cycloidal phase to the cone phase is indeed suppressed by pressure.

In order to analyse the data shown in figures 1(*c*) and 2(*c*), we may describe the magnetic moment configuration of the Er atoms at r_n in the nth basal plane of the modulated structure as follows:

$$\begin{aligned}
\mu_x(r_n) &= \mu_{x0}\cos(r_n \cdot Q + \alpha_x) \\
\mu_y(r_n) &= \mu_{y0}\cos(r_n \cdot Q + \alpha_y) \sim 0 \\
\mu_z(r_n) &= A_1\cos(r_n \cdot Q + \gamma_1) + A_3\cos(3r_n \cdot Q + \gamma_3) + A_5\cos(5r_n \cdot Q + \gamma_5) \\
&\quad + A_7\cos(7r_n \cdot Q + \gamma_7)
\end{aligned} \tag{1}$$

or

$$\begin{aligned}
\mu_x(r_n) &= \mu_0\cos(r_n \cdot Q + \beta_0) \\
\mu_y(r_n) &= \mu_0\sin(r_n \cdot Q + \beta_0) \\
\mu_z(r_n) &= A_1\cos(r_n \cdot Q + \gamma_1) + A_3\cos(3r_n \cdot Q + \gamma_3) + A_5\cos(5r_n \cdot Q + \gamma_5) \\
&\quad + A_7\cos(7r_n \cdot Q + \gamma_7)
\end{aligned} \tag{2}$$

where x, y, and z refer to moment components along the a-, b-, and c-directions of the real space lattice. The modulation vector $Q = (\frac{2}{7}2\pi/c)\hat{c}$, and the moment components μ_{x0}, μ_{y0}, and μ_0 are perpendicular to c, while A_i (i = 1, 3, 5 and 7) are parallel to c. For suitable choices of amplitudes and phases, equations (1) and (2) describe cycloidal and c-axis modulated helical orderings, respectively, and are equivalent to special cases of the generalized strucutre described by Fujii *et al* (1981).

The data presented in figures 1(*c*) and 2(*c*) may be analysed in terms of either of the structures defined above, and the intensities of the magnetic satellites are directly related to the magnetic amplitudes (μ_{x0}, μ_{y0}, μ_0, A_i with i = 1, 3, 5, 7) defined in equations (1) and (2). The results of these analyses are summarized in table 1. The table lists the moment components of the cycloidal structure of Er at 4.5 K and 11.5 kbar hydrostatic pressure in the notation of equations (1) and (2), together with the moments determined at ambient pressure by Habenschuss *et al* (1974). The moment components determined at 4.5 K and 11.5 kbar show reasonable agreement with those of the cycloidal structure at 22 K and ambient pressure, although the higher-harmonic moment components perpendicular to the c-axis are not observed for the magnetic structure at 4.5 K and 11.5 kbar hydrostatic pressure.

We have attempted to estimate the phases, α_x, α_y, β_0 and γ_i, where i = 1, 3, 5 and 7, between the individual moment components in equations (1) and (2) by a trial and error method with the following conditions:

(1) Within the experimental uncertainties the total moment on any atom i should not exceed the free ion value of 9 μ_B per Er atom.

(2) The moments of all atoms should be as large and of as equal length as possible (Forgan 1992).

(3) μ_{y0}, which causes the plane of the cycloidal spin configuration to wobble, is assumed to be negligible.

Table 1. Comparison between the magnetic structure of Er at 4.5 K and 11.5 kbar hydrostatic pressure and those at ambient pressure (Habenschuss *et al* 1974). The moment component and the modulation vector q are in units of the Bohr magneton (μ_B) and $2\pi/c$, respectively. The estimated uncertainties of the moment components for the present data are given by the number in parentheses in the first column.

11.5 kbar, 4.5 K Cycloid Present work	Ambient, 4.5 K Cone Habenschuss *et al* (1974)	Ambient, 22 K Cycloid Habenschuss *et al* (1974)
$\mu_{x0} = 4.41(0.34)$	$\mu_0 = 4.44$	$\mu^1_{x0} = 5.4$
$\mu_{y0} \simeq 0$ (assumed)	$A_1 = 7.8$	$\mu^n_{x0} \neq 0,\ n = 3, 5$
$A_1 = 10.16\ (0.64)$	$A_n = 0,\ n = 3,....$	$\mu_{y0} \simeq 0$
$A_3 = 3.33\ (0.06)$		$A_1 = 10.5$
$A_5 = 2.67\ (0.07)$		$A_3 = 2.5$
$A_7 = 1.83\ (0.24)$		$A_5 = 1.2$
		$A_7 = 0.8$
	$\mu_{total} = 9.0$	$A_n,\ n =$ odd, up to 17
$\mu_\perp = 3.12(0.24)$[a]		$\mu^1_\perp = 3.8$[a]
		$\mu^n_\perp \neq 0,\ n = 3, 5$
$q \simeq 2/7$	$q \simeq 5/21$	$q \simeq 2/8$

[a] For the helical structure $\mu_\perp = \frac{1}{\sqrt{2}}\mu_{x0}$

Table 2. Phases determined by the method described in section 3. The notation is the same as that used in equations (1) and (2), and the corresponding spin configurations are shown in figures 4(*a*), 4(*c*) and 4(*d*). The phases for the helical structure shown in figure 5 are identical to the phases for the cycloidal structure shown in figure 4(*a*) ($\beta_0 = \alpha_x$).

11.5 kbar, 4.5 K Cycloid, figure 4(*a*) Present work	Ambient, 22 K Cycloid, figure 4(*c*) Habenschuss *et al* (1974)	Ambient, 22 K Cycloid, figure 4(*d*) Habenschuss *et al* (1974)
$\alpha_x = \pi/2$	$\alpha_x = -\pi/4$	$\alpha_x = \pi/8$
$\gamma_1 = 0$	$\gamma_1 = \pi/4$	$\gamma_1 = -3\pi/8$
$\gamma_3 = \pi$	$\gamma_3 = -\pi/4$	$\gamma_3 = -\pi/8$
$\gamma_5 = 0$	$\gamma_5 = 5\pi/4$	$\gamma_5 = \pi/8$
$\gamma_7 = \pi$	$\gamma_7 = -5\pi/4$	$\gamma_7 = -5\pi/8$
$q \simeq 2/7$	$q \simeq 2/8$	$q \simeq 2/8$

The results of these estimates are shown in figures 4 and 5, and the resulting phases are quoted in table 2. Figure 4(*a*) shows the spin configuration of a cycloidal structure given by equation (1) for Er at 4.5 K and 11.5 kbar hydrostatic pressure. For comparison, figure 4(*b*) shows the moment-configuration derived by Cowley and Jensen (1992) for Er at ambient pressure and 49 K. It is important to recognize that, because the structure of Er at 11.5 kbar hydrostatic pressure is commensurate, we measure the ferromagnetic component directly. This means that the phase of the seventh harmonic is not a free parameter; it must be either 0 or π. Therefore, although a structure with phases $\pi/2$, 0, π, 0, $2\pi/3$ fulfills the three conditions listed above, the corresponding structure is not the correct commensurate structure because the ferromagnetic moment component will be too small ($A_7 \cos(2\pi/3)$ instead of A_7). The above choice of phases cannot be excluded *a priori* for an incommensurate modulation. However, it will not lead to a very plausible structure, because for an

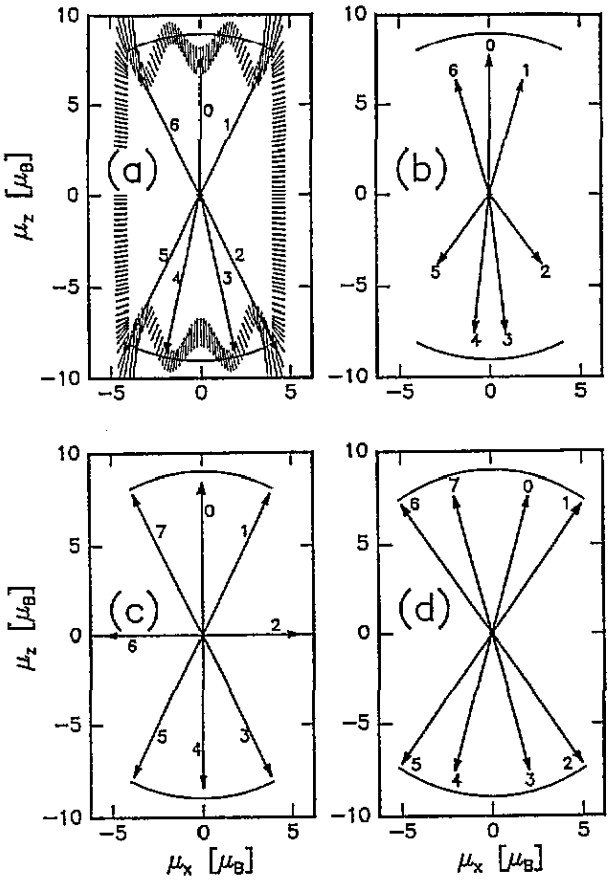

Figure 4. Spin configuration for a cycloidal structure of Er at 4.5 K and at 11.5 kbar hydrostatic pressure determined as described in the text. The moments have been projected onto the xz-plane and displaced to a common origin. The numbers i = 0, 1, 2, ..., 6 (, 7) refer to spins in the ith layer of atoms. The moment components along the y-axis were assumed to be zero. The two arcs mark the 9 μ_B upper limits of the total Er moment per atom. The borders of the hatched areas in figure 4(*a*) are given by the two curves calculated for an incommensurate structure by using the upper and lower limits for the ordered moment amplitudes defined by the uncertainties quoted in the first column of table 1. Figures 4(*c*) and 4(*d*) show similar diagrams derived for Er at 22 K and at ambient pressure using the parameters of Habenschuss *et al* (1974). Figure 4(*b*) shows the spin configuration for Er at ambient pressure and 49 K derived by Cowley and Jensen (1992). (See tables 2 and 3 for details.)

incommensurate structure with the same harmonic components as the commensurate structure, the spins in neighbouring layers will vary in a rather erratic way and in some layers perpendicular to the c-axis the spin may dramatically exceed the free ion value for Er. For completeness, figures 5(*a*) and 5(*b*) show the spin configurations in the xz- and yz-planes assuming a c-axis modulated helical structure (equation (2)) for Er at 4.5 K and 11.5 kbar hydrostatic pressure. The resulting phases are also listed in table 2.

The data of Habenschuss *et al* (1974) for Er at 22 K and at ambient pressure

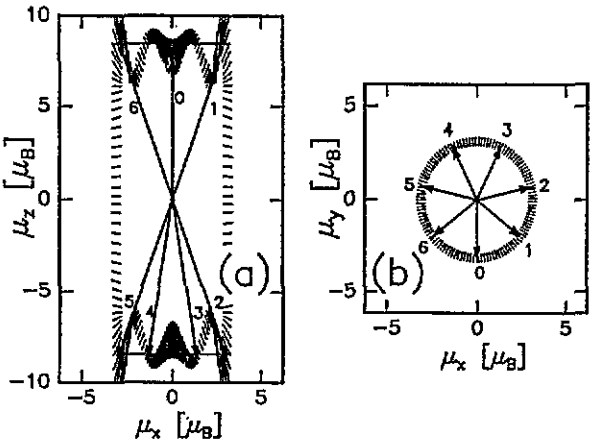

Figure 5. Moment configuration for a c-axis modulated helical structure of Er at 4.5 K and at 11.5 kbar hydrostatic pressure determined as described in the text. The moments have been projected onto the xz-plane (*a*) or xy-plane (*b*) and displaced to a common origin. The numbers i = 0, 1, 2, ..., 6 refer to spins in the ith layer of atoms. The thin lines in figure 5(*a*) mark the upper limits of the Er moment per atom in the xz-plane for a basal plane moment component of 3.12 μ_B and a total Er moment of 9 μ_B. The borders of the hatched areas in figures 5(*a*) and 5(*b*) are given by the curves calculated for an incommensurate structure by using the upper and lower limits for the ordered moment amplitudes defined by the uncertainties quoted in the first column of table 1.

have been analysed in the same way as our data at 11.5 kbar hydrostatic pressure, and two possible spin configurations are shown in figures 4(*c*) and 4(*d*). From the neutron diffraction data alone, it is impossible to decide which of these two structures is the correct structure of Er at 22 K and ambient pressure. For the highly anisotropic structure shown in figure 4(*c*), the spins in the second and sixth layers lie entirely in the basal plane while the remaining spins lie predominantly along the *c*-axis. Because of the strong magnetoelastic couplings in Er (Jensen and Mackintosh 1991) this configuration will lead to lattice distortions with a periodicity of q = 4/8. In contrast, the structure shown in figure 4(*d*) is relatively isotropic with all spins predominantly along the *c*-axis and will presumably only accommodate relatively small lattice distortions. Therefore, precise x-ray diffraction intensity measurements may allow us to distinguish between these two structures. Some years ago, Gibbs *et al* (1986) made combined neutron and x-ray diffractions of Er. In these studies, lattice modulations with q = 4/8 were indeed observed. However, they did not report any details about the corresponding intensities. Therefore, it is presently not possible to estimate which of the structures shown in figures 4(*c*) and 4(*d*) are the correct structure for Er at ambient pressure and 22 K.

The moment components on the atoms in the seven-layer cycloidal structure at 4.5 K and 11.5 kbar hydrostatic pressure are listed in table 3 together with the uncertainties (in parentheses) estimated from the borders of the hatched area in figure 4(*a*) (see also the figure caption for figure 4). The cycloidal structure of figure 4(*a*) and table 3 has a c-axis net moment of (−1.8 ± 0.3) μ_B per layer of Er atoms. The maximum deviation from the *c*-axis of a spin is ~ 26° and the structure is almost a three-up-four-down structure similar to the one observed in Tm metal

by Koehler *et al* (1962). In Tm, the spins in planes perpendicular to the c-axis are ferromagnetically aligned parallel to the c-axis in a three-up-four-down sequence with modulation vector $q = 2/7$ along the c-axis. For completeness it should be mentioned that a c-axis magnetic field (Lin *et al* 1992) tends to stabilise the $q = 2/7$ phase in Er, at least for fields below 1.5 T. For fields above 1.5 T the $q = 2/7$ is rapidly destabilized with a tendency towards stabilization of the $q = 6/21$ for fields above 2.5 T.

Table 3. Moment components in Bohr magnetons (μ_B) determined by the method described in section 3. The notation is the same as that used in equation (1), and the corresponding spin configurations are shown in figure 4. The data quoted for Er at ambient pressure and 49 K are calculated by Cowley and Jensen (1992) with $\mu_i(n) = gJ_i(n)$ ($i = x, y, z$). For simplicity $\mu_y(n) \simeq 0$ for all spin configurations. The numbers in parentheses in the first section of the table are the estimated uncertainties in the last digits (see the text and the figure caption for figure 4). The signs before μ_{total} correspond to the signs of the c-axis components.

11.5 kbar, 4.5 K, figure 4(*a*); Present work; $q \simeq 2/7$

Layer No n	$\mu_x(n)$	$\mu_z(n)$	$\mu_{total}(n)$
0	0.0	7.7(1.0)	7.7(1.0)
1	3.5(3)	6.9(6)	7.7(7)
2	4.3(3)	−8.6(5)	−9.6(6)
3	1.9(1)	−8.6(8)	−8.8(8)
4	−1.9(1)	−8.6(8)	−8.8(8)
5	−4.3(3)	−8.6(5)	−9.6(6)
6	−3.5(3)	6.9(6)	7.7(7)
Mean μ_z/layer along z^+		7.2(4)	
Mean μ_z/layer along z^-		−8.6(3)	
Net μ_z/layer		−1.83(26)	

Ambient, 49 K, figure 4(*b*); Cowley and Jensen (1992); $q \simeq 2/7$

Layer No n	$\mu_x(n)$	$\mu_z(n)$	$\mu_{total}(n)$
0	0	7.69	7.69
1	1.87	6.33	6.60
2	2.89	−3.75	−4.73
3	0.88	−7.47	−7.52
4	−0.88	−7.47	−7.52
5	−2.89	−3.75	−4.73
6	−1.87	6.33	6.60
Mean μ_z/layer along z^+		6.78	
Mean μ_z/layer along z^-		5.61	
Net μ_z/layer		−0.30	

Ambient, 22 K, figure 4(*c*); Habenschuss *et al* (1974); $q \simeq 2/8$

Layer No n	$\mu_x(n)$	$\mu_z(n)$	$\mu_{total}(n)$
0	0	8.4	8.4
1	3.8	7.8	8.3
2	5.4	0	3.8
3	3.8	−7.8	−8.3
4	0	−8.4	−8.4
5	−3.8	−7.8	−8.3
6	−5.4	0	−3.8
7	−3.8	7.8	8.3
Mean μ_z/layer along z^+		6.0	
Mean μ_z/layer along z^-		−6.0	
Net μ_z/layer		0.0	

Ambient, 22 K, figure 4(*d*); Habenschuss *et al* (1974); $q \simeq 2/8$

Layer No n	$\mu_x(n)$	$\mu_z(n)$	$\mu_{total}(n)$
0	2.1	7.5	7.7
1	5.0	7.1	7.9
2	5.0	−7.1	−7.9
3	2.1	−7.5	−7.7
4	−2.1	−7.5	−7.7
5	−5.0	−7.1	−7.9
6	−5.0	7.1	7.9
7	−2.1	7.5	7.7
Mean μ_z/layer along z^+		7.8	
Mean μ_z/layer along z^-		−7.8	
Net μ_z/layer		0.0	

It may be noted that, although the analysis results in different moments on the atoms in the seven-layer structure, the data are (within the experimental uncertainties)

consistent with a structure having three atoms with moments of equal lengths ((7.7±0.5) μ_B/layer) and positive c-axis component, and four atoms with moments of equal, somewhat larger length ((−9.2±0.4) μ_B/layer) with negative c-axis component. However, if we compare the cycloidal structure of Cowley and Jensen (1992) at ambient pressure and 49 K (figure 4(*b*)) with the structure found at 11.5 kbar hydrostatic pressure and 4.5 K (figure 4(*a*)), it is apparent that the latter is just a squared-up version of the former with a considerably larger net moment along the negative c-axis: (−1.8 ± 0.3) μ_B/layer as compared to −0.3 μ_B/layer. The two structures found at ambient pressure and 22 K when analysing the data of Habenschuss *et al* (1974) have no net c-axis moment. Presumably, the cycloidal structure shown in figure 4(*d*) is (within the experimental uncertainties) consistent with eight spins of equal length, four with positive and four with negative c-axis components, i.e. a double fan.

4. Conclusions

The present neutron diffraction studies of the magnetic structures of erbium metal at 4.5 K and 11.5 kbar hydrostatic pressure show that the transition to a conical structure at low temperatures is suppressed and that the cycloidal structure, with modulation vector $Q \simeq (\frac{2}{7}2\pi/c)c$ and with higher harmonics of the c-axis moment component, persists down to 4.5 K. The available experimental data do not allow us unambiguously to distinguish between the three-domain cycloidal and the c-axis modulated helical structure. However, a recent calculation of Jensen (1992) indicates that, although the energy differences are marginal, the cycloidal structure is energetically more favourable than the c-axis modulated helical structure even below 20 K. Despite the ambiguity in the neutron-diffraction data we therefore conclude that the c-axis modulated cycloidal structure is the most likely magnetic structure in Er at 4.5 K and 11.5 kbar hydrostatic pressure. However, within the accuracy of our experimental data, we are unable to determine the wobbling of the cycloid. Our conclusion is not only supported by Jensen's (1992) calculations, but may also be substantiated by the measurements at ambient pressure of Cowley and Jensen (1992) which show that when the basal plane moment component in Er starts to order, the length of the modulation vector of this component is locked to the same value as the modulation vector of the c-axis ordered moment component. Although this experimental fact does not exclude a c-axis modulated helical structure it is unlikely that such a structure would have identical periodicities for the two very differently ordered moment components. However, for a cycloidal structure the basal plane ordering would be induced by the c-axis ordering with a strong incipient coupling between the c-axis and the basal plane moment components and, consequently, the periodicities for the two moment components would be identical.

An interesting result of Jensen's (1992) numerical calculations is that below 17 K the anisotropy may cause the average cycloidal structure to tilt out of the xz-plane. In other words, the spins will wobble around a plane which is tilted away from the ac-plane of the HCP structure and form a structure with wobbling non-constant moment components in the basal plane. The expected wobbling of the cycloidal structure is not caused by the trigonal coupling alone (Cowley and Jensen 1992) and is also considerably larger than that observed in Er at ambient pressure. Presumably it will be difficult to distinguish between the tilted and non-tilted cycloidal structures by

neutron diffraction, at least with the accuracy of the presently available data, but the transition between the tilted and non-tilted cycloid may perhaps be observed as a second-order transition in heat capacity measurements under applied pressure.

The fact that the $q = 2/7$ cycloidal structure persists down to low temperature under 11.5 kbar hydrostatic pressure and the transition to the $q = 2/8$ cycloidal structure is suppressed, at least below 4.5 K, is somewhat unexpected. However, the quenching of the cone phase is consistent with the estimate of Jensen and Mackintosh (1991) that a hydrostatic pressure of 2.5 kbar should be sufficient to quench this phase. Therefore, neutron diffraction measurements of Er at 4.5 K and lower pressures than 11.5 kbar can be expected to give useful information about the two-ion magnetoelastic couplings which are responsible for the quenching of the cone phase (Jensen and Mackintosh 1991). The temperature dependence of the magnetic structure of Er under pressure is also quite interesting: first of all, because initial permeability measurements under pressure suggest the existence of a new intermediate phase around 25 K (Milton and Scott 1967); secondly, because of the possible existence of a tilted cycloidal structure below 17 K (Jensen 1992) and thirdly, because preliminary, relatively inaccurate, neutron diffraction data for the temperature dependence of the $(1\ 1\ 0)^{+q}$ intensity at 11.5 kbar hydrostatic pressure show no strong anomalies at these temperatures. From the data for the temperature dependence, we may only conclude that the cycloidal structure changes to a longitudinally c-axis modulated structure at $\sim$ 50 K and that the modulation vector remains unchanged between 4.5 K and $\sim$ 50 K, where it tends to increase. The intensities of the magnetic satellites originating from the higher harmonics of the c-axis moment component which are observed at 4.5 K (see figure 2(c)) decrease slowly with increasing temperature, although they remain visible up to $\sim$ 60 K. However, more precise neutron diffraction experiments as a function of temperature and pressure are needed for a more complete understanding of the structure of Er under hydrostatic pressure.

Acknowledgments

The authors gratefully acknowledge stimulating discussions with J Jensen and A R Mackintosh. Special thanks are due to J Jensen for permitting us to quote the results of his calculations and use them in table 3 and figure 4(b).

The high-pressure cell used for the present work has been developed under the auspices of the US–Japan Cooperative Program in Neutron Scattering supported by the US Department of Energy and the Ministry of Education, Science and Culture, Japan.

References

Achiwa N, Kawano S, Onodera A and Nakai Y 1988 *J. Physique Coll.* **49** C8 349
Atoji M 1974 *Solid State Commun.* **14** 1047
Cowley R A and Jensen J 1992 *J. Phys.: Condens. Matter* **4** 9673
Forgan E M 1992 *J. Magn. Magn. Mater.* **104–7** 1485
Gibbs D, Bohr J, Axe J D, Moncton D E and D'Amico K L 1986 *Phys. Rev.* B **34** 8182
Fujii H, Hashimoto Y, Okamoto T, Achiwa N and Kawano S 1981 *J. Phys. Soc. Japan* **50** 2939
Habenschuss H, Stassis C, Sinha S K, Deckman H D and Spedding F H 1974 *Phys. Rev.* B **10** 1020
Jensen J 1976 *J. Phys. F: Met. Phys.* **6** 1145
Jensen J 1992 private communication

Jensen J and Mackintosh A R 1991 *Rare Earth Magnetism: Structures and Excitations* (Oxford: Clarendon)
Kawano S, Achiwa N, Onodera A and Nakai Y 1992 *Physica* B **180** & **181** 46
Koehler W C, Cable J W, Wollan E O and Wilkinson M K 1962 *Phys. Rev.* **126** 1672
Lin H, Collins M F, Holden T M and Wei W 1992 *Phys. Rev.* B **45** 12 873
McWhan D B, Bloch D and Parisot G 1974 *Rev. Sci. Instrum.* **45** 643
McWhan D B and Stevens A L 1965 *Phys. Rev.* **139** A682
Milton J E and Scott T A 1967 *Phys. Rev.* **160** 387
Onodera A, Nakai Y, Kunitomi N, Pringle O A, Smith H G, Nicklow R M, Moon R M, Amita F, Yamamoto N, Kawano S, Achiwa N and Endoh Y 1987 *Japan. J. Appl. Phys.* **26** 152
Robinson L B, Tan S and Sterrett K F 1966 *Phys. Rev.* **141** 548
Umebayashi H, Shirane G, Frazer B C and Daniels W B 1968 *Phys. Rev.* **165** 688
Wazzan A R, Vitt R S and Robinson L B 1967 *Phys. Rev.* **159** 400